Hybrid organic–inorganic PMMA optical fibers functionalized with photochromic active WO3 nanoparticles: from materials design to photochromic fabrics

Yazan Badour, Matthieu Pedros, Manuel Gaudon, Sylvain Danto

Hybrid Organic–Inorganic PMMA Optical Fibers Functionalized with Photochromic Active WO_3 Nanoparticles: From Materials Design to Photochromic Fabrics

*Yazan Badour, Matthieu Pedros, Manuel Gaudon, and Sylvain Danto**

Here, the direct incorporation of photochromic WO_3 nanoparticles is investigated in a matrix of polymethyl methacrylate (PMMA) by bulk radical polymerization for the fabrication of plastic optical fibers (POFs). All the prepared composites, from preforms to 1D single fibers and 2D fabrics, are thoroughly investigated, leading to insight into their thermal, morphological, and photochromic properties (coloring/bleaching amplitudes and kinetics). It is found that the preforms exhibit partially irreversible photochromic behavior, whereas the single fibers proved to be effectively reversibly photochromic through a degradation of transmission signal upon UV irradiation and a full recovery under dark conditions. The as-prepared PMMA plastic fibers, both undoped and doped, show good homogeneity without any imperfections or contamination. The WO_3 nanoparticles play a dual role as intrinsic and extrinsic absorption centres leading to higher transmission losses. Finally, a hand-made textile woven with a bundle of doped fibers is presented. The proposed 1D single fibers and 2D fabrics demonstrate their great potential as novel hybrid inorganic–organic materials in the domain of flexible UV-sensors and photochromic smart textile with improved color stability and lifetime.

1. Introduction

The combination of organic and inorganic materials at molecular or nanometric level provide an extensive field of research in material science for developing novel multifunctional devices.[1,2] Generally, inorganic compounds exhibit thermal stability, high strength, and rich coordination chemistry. On the other hand, organic compounds offer a wide range of possibilities to elaborate devices based on their versatile chemical and physical properties, chemical compositions, and straightforward processing techniques.[3–6] Polymeric optical fibers (POFs) represent a remarkable class of organic host in comparison with standard inorganic glass optical fibers thanks to their higher flexibility, elastic strain limits, and fracture toughness.[7] POFs are made out of various types of polymers, including polystyrene (PS),[8] amorphous fluorinated polymers (CYTOP),[9] polyethersulphone (PES),[10] or polycarbonate (PC).[11] Poly(methyl methacrylate) (PMMA) is also widely considered as a replacement of inorganic glass for the elaboration of POF, thanks to its higher chemical, photochemical stability, durability, and scratch resistance. Optical fibers made of pure PMMA polymer are mainly employed to date for sensing, short-distance optical links,[12–14] or smart textiles.[15]

Traditional methods to color textile with organic dyes based on impregnation own several disadvantages such as color fading or inhomogeneities due to alterations in dye uptake and distribution, or even toxicity issues due to the delamination of the dye from the surface of the fibers.[16] In contrast, the integration of active compounds within the polymer matrix could lead to a more uniform distribution and protection by encapsulation of the material.[17] The low manufacturing temperature of POFs compared to inorganic glass fibers permits to embed a wide range of dopants in the fiber matrix, mostly organic dyes and conjugated polymers.[18–22] For instance P. Miluski et al. have shown fluorescence emission tuning in PMMA fibers doped with Bis-MSD (1,4-bis(2-methylstyryl) benzene) dye.[23] The luminescent emission in PMMA samples co-doped by trivalent rare earth elements was also reported.[24,25] The main elaboration methods to embed the doping elements within the PMMA matrix consist of adding the dopants to the monomer mixture during the pre-polymerization step,[26] the direct mechanical mixing of the dopants with the melted PMMA during the extrusion process[27] or in soaking the dopant molecules into the microstructure fiber using the solution-doping method.[28]

Y. Badour, M. Gaudon, S. Danto
Centre National de la Recherche Scientifique (CNRS)
Université de Bordeaux
Bordeaux INP, ICMCB (UMR 5026), Pessac F-33600, France
E-mail: sylvain.danto@u-bordeaux.fr
M. Pedros
Département Science et Génie Matériaux SGM IUT
Université Bordeaux
Bordeaux F-33175, France

The ORCID identification number(s) for the author(s) of this article can be found under https://doi.org/10.1002/XXXXXXXXXXXXX

DOI: 10.1002/XXXXXXXXXXXXX

In our work, we present a new class of transparent PMMA fibers doped with transition metal oxide-based photochromic materials, namely tungsten oxide compounds (WO_3), for X-chromic applications. X-chromic materials represent a compelling class of dopants as they can change reversibly their optical properties under the effect of an external stimulus, such as temperature, voltage, atmosphere, photochromism exhibiting a reversible change in optical properties through the action of light.[29,30] To date, photochromic phenomena in POF and in color-changing UV-sensitive textured yarns have relied vastly on organic photochromic materials.[31,32] The photochromic activity of WO_3 shows significant features such as the response to visible light and improved photochromic kinetics.[33–36] Photochromic WO_3 shaped as thin films,[33,35–38] nanocubes,[39] nanowires,[40] or nanoflakes[41] were reported and thoroughly investigated in the last decade, but very few were devoted to organic-WO_3 hybrids.[42,43]

Although these nanocomposite materials based on WO_3 have been thoroughly investigated and have been used as photochromic film devices, researches are mainly focused on photochromic composite films, photochromic fibers based on WO_3 are rarely reported. While there has been a significant amount of research done on the synthesis and applications of WO_3 nanoparticles, the integration of WO_3 into microfibers remains a relatively unexplored field. One possible reason is the difficulty to achieve uniform dispersion of WO_3 nanoparticles within the fibers. Their weak stability under basic and acidic conditions represents another limitation. The photochromic qualities of WO_3, which are influenced by environmental conditions including humidity and temperature, provide another difficulty when using WO_3 as a cladding or soaking dye on microfibers.

In the following, the bulk PMMA preforms were prepared by free radical pre-polymerization in the presence of WO_3 nanoparticles with three different doping concentrations (0%, 0.2%, and 0.5% in weight). The primary objective of this study is to optimize the dispersion of WO_3 nanoparticles within the monomer matrix, followed by the implementation of bulk rod polymerization techniques. The ultimate goal is to fabricate meticulously designed functional polymeric preforms. This approach is crucial for achieving a uniformly dispersed matrix, required to meet two critical requirements: first, ensuring that the composite polymer maintains optical transparency, and second, achieving a significant optical contrast before and after irradiation. In contrast to mechanical mixing procedures, which need significant energy input and material consumption to satisfy the minimal batch size for machine processing, free radical polymerization provides a distinct benefit. This approach allows for direct doping of photochromic nanoparticles into polymer chains, using only a small amount of the nanoparticles. Notably, this methodology eliminates worries about contamination and microdispersion that are typical in competing procedures (for example extrusion).

The first part addressed the rheological properties of the produced polymeric preforms. Also, we discuss the photochromic properties of the various proposed systems as preforms, optical fibers, and fabrics. Integrating WO_3 photochromic NPs in the PMMA matrix would greatly improve color stability and resistance to environmental factors such as UV radiation and humidity over typical dyed textiles.

2. Experimental Section

2.1. Synthesis and Shaping of the WO_3-PMMA Composites

2.1.1. Synthesis of the WO_3 Powders

All chemical reagents were purchased from Sigma–Aldrich. Tungsten (VI) chloride was used as tungsten source, and diethylene glycol (DEG) as solvent. WCl_6 (7.2 g) was added to 100 mL of DEG and 20 mL of distilled water. The mixture was heated at 180 °C under continuous stirring and refluxed for 3 h. At the end of the reaction, a deep blue precipitate was obtained. It was washed and centrifuged with ethanol to remove any traces of solvent and dried in an oven at 80 °C for 24 h. To functionalize the surface of the powder by phosphonic groups, a 150 mg of tert-butylphosphonic acid (98%, $tBuPO_3H_2$) was dissolved in 5 mL of ethanol then added (drop by drop) to a separated batch of 250 mg of WO_3 dispersed in 25 mL of ethanol. The mixture was stirred for 24 h at room temperature then washed three times by ethanol. The modified powder was obtained after a drying step for 48 h.

2.1.2. Composite Preform Preparation

The co-doped PMMA preforms were fabricated using methyl methacrylate (MMA, 99%) monomers, benzoyl peroxide (BP, 70%), sodium hydroxide (NaOH, 98%) and WO_3 as the doping agent. First, the monomer stabilizer (inhibitor) was removed by washing with a 1 M NaOH solution for several time. Following, the MMA was distilled and double-dried using column chromatography to remove any traces of water or moistures. Different amounts of surface-modified WO_3 nanoparticles (0, 0.2, and 0.5% wt.) and MMA were placed into sealed pyrex tubes (12 mm in diameter). The dispersions were sonicated for 30 min and kept for 10 h in the dispersed state to achieve a complete wetting of the particle surface. For each solution a 0.5% wt. of BP was added to initiate the radical polymerization in the tube. The polymerization was performed at 70 °C for 24 h under argon atmosphere. The rod-like preforms were obtained after breaking the glass tube. Finally, the preforms were kept for 10 days in vacuum oven to ensure the complete drying of the preforms prior to the drawing step. Three different preforms with WO_3 doping of 0, 0.2, and 0.5% wt., labeled as PM00, PM02, and PM05 respectively, were prepared following this process, illustrated in **Figure 1**.

2.1.3. Composite 1D Fiber Drawing

The plastic optical fibers were drawn using a 3-meter-high optical fiber drawing tower with an annular electrical furnace having a sharp temperature profile. The plastic preforms were heated up above glass transition temperature T_g at 20 °C.min^{-1} to initiate the elongation process. Once the drop formed and tied on the drum, the preforms were slowly fed into the furnace while continuously monitoring the drawing parameters (temperature, drum velocity, feed rate, tension, diameter). Following this procedure, preforms were successfully drawn into hundreds of meters-long fibers with diameters ranging from 100 to 660 µm. The process was performed under an argon gas flow (2 L.min^{-1}) to avoid

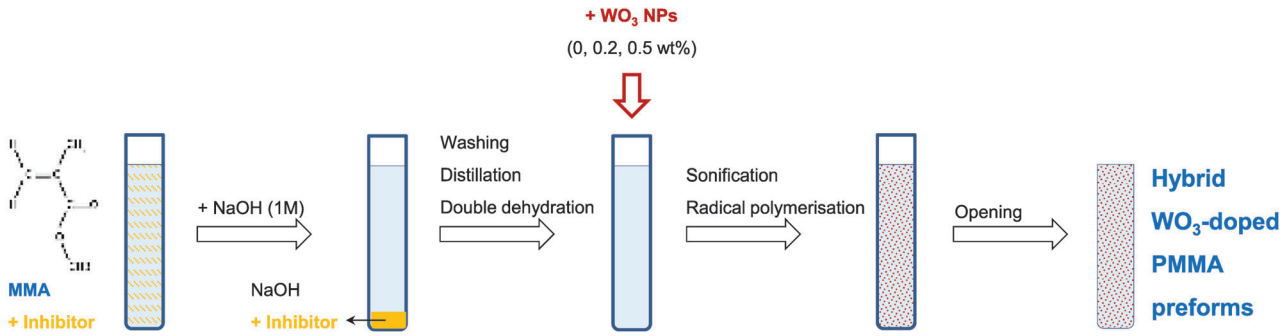

Figure 1. Road map of the used techniques to elaborate the lab-made preform.

any external pollution of the preform surface. The fibers prepared from the preforms PM00, PM02, and PM05 were labeled as FPM00, FPM02, and FPM05 respectively.

2.1.4. Composite 2D Textile Preparation

Photochromic pieces of FPM02 fibers were woven manually into a fabric with dimension 2×2 cm^2 to produced as prototypic textile object.

2.2. Characterization Techniques

2.2.1. Dynamic Light Scattering (DLS)

Dynamic light scattering (DLS) was used to determine the size distribution profile of the NPs in the monomer with a VASCOTM nanoparticle size analyzer. Real-time signal acquisitions were performed every 30 s if the noise of the signal did not exceed 1.06%, and 8% acquisitions were accomplished during 16 min in total. Size distributions of the nanoparticles in MMA were analyzed by the Cumulant algorithm (assuming monodisperse dispersion), provided by NanoQ software. The acquisition temperature for all measurements was fixed automatically by the device at 20 °C.

2.2.2. Glass Transition Temperatures

Glass transition temperatures (T_g) were determined using a Shimadzu DSC-50 differential scanning calorimeter with a precision of ±2 °C and a 10 °C min^{-1} heating rate. 50 mg of polymer samples were placed in a platinum crucible while a second empty platinum crucible was used as a reference sample. The T_g was determined as the onset of the thermal phenomena from the tangent intersection of the DSC curves.

2.2.3. Melt Flow Index

Melt Flow Index (MFI) was measured according to the ASTM D1238 standard using the Dynisco Polymer Test Model. Prior to measurement the prepared cylindrical preforms were cut into small pieces to facilitate its loading into the melt indexer machine (MIM) entrance. The MIM was preheated at 130 °C for ≈30 min and then 5 g of the PMMA/WO_3 mixture were loaded in the MIM. A weight load of 2.2 kg was set up on the piston, and a stopwatch was used to monitor the weight of the extruded filament in 10 mns.

2.2.4. Electronic Microscopy

The surface morphologies of the as-prepared preforms and fibers were observed by scanning electron microscopy (SEM) using a TESCAN Vega II SBH microscope and JEOL JSM-6700F and by high-resolution transmission electron microscopy (HRTEM, JEOL 2200FS, operating at 200 kV). High-resolution transmission electron microscopy (HR-TEM) was performed using a JEM-2100 transmission electron microscope. Prior to TEM observation, ultrathin sections (75 nm thick) were cut using a Boeckeler Power Tome XL microtome.

2.2.5. Optical Characterizations

The photochromic properties of all the samples were tested using the same 8 W UV lamp (λ = 365 nm) for producing the composite coloration. Photochromic properties for preforms and fabric were characterized using UV–vis diffuse reflectance spectroscopy, from 200 to 2000 nm, equipped with an integration sphere (spectral resolution: 1 nm and band length: 2 nm) mounted on the Cary 5000 spectrophotometer. Halon was used as a white reference. A 1 mm-thick slice cut from the PM02 preform and the woven fabric (2×2 cm^2) of FPM02 fibers were placed on a white background for measurements. The photochromic properties of single fibers were tested through measurements of the axial transmission of 5 cm-long length fibers. RGB space colorimetric parameters were determined from the spectra using a two-step mathematic treatment. The first step consists in extracting the XYZ tri-stimulus values (defined by the CIE, 1964) from the integration (over the visible range, i.e., from λ = 380 nm up to 780 nm) of the product of $x(\lambda)$, $y(\lambda)$, or $z(\lambda)$ functions (CIE-1964) with the diffuse reflectance spectra function $X = \int x(\lambda).R(\lambda).d\lambda$. Then, the transfer equations (defined by the CIE, 1976) were used to transform the XYZ space to the L*, a*, and b* common three-color space parameters.

For the axial transmission spectra through the single fibers, a 100 W halogen broadband source, and an optical spectrum analyzer were employed to collect the data. The calculation of the

attenuation coefficient was averaged from measurements on 1, 0.75, and 0.5 m-long fibers with a diameter of ≈350 µm. The end facets of each measured fiber were carefully polished prior to measurements to ensure a proper light coupling efficiency. The fibers were kept straight during measurements to avoid any bending losses.

3. Results and Discussion

3.1. WO_3 Particle Size Distribution into Monomer Suspensions

The particles are hydrophobized by surface modification with (tBuPO3H2), which is required to block the formation of aggregates and to increase the wettability by the monomer and polymer.[44] DLS measurements were used to track the size variation of the NPs as a result of the surface modification of WO_3 by phosphonic acid groups in the monomer solution before the polymerization. Three samples were investigated: 0% wt. WO_3, 0.2% wt. WO_3, and 0.5% wt. WO_3. The DLS indicates a clear decrease in the average size as a result of surface modification. The average size drops from 632 nm with polydispersity index (PDI = 0.72) in the 0.2% wt. WO_3 (un-modified) in MMA to 38 nm (PDI = 0.35) in 0.2% wt. WO_3 (modified). Comparing the two functionalized-particle samples, increasing the particle content to 0.5% wt. (average size of 42 nm, PDI = 0.16) does not cause aggregation in the monomer recording almost the same distribution as the 0.2% wt. sample.

3.2. Composite Prefrom Characterizations

3.2.1. Thermal Behavior

The thermal behavior of the prepared PMMA preforms doped with different concentrations of WO_3 (0% wt., 0.2% wt., and 0.5% wt.) was studied with the means of differential scanning calorimetry (DSC) (**Figure 2**). The DSC thermograms of undoped and doped PMMA preforms exhibit similar thermal behavior with a clear transition centered on 90°C, which is attributed to the glass transition temperature typical of PMMA polymer.[44]

The values of T_g are resumed in **Table 1**. For comparison purpose, we also included the T_g of a commercially available PMMA, labeled as PMCom. PM00 shows a T_g (86.5 °C) close to the one of the commercial PMCom (90.4 °C). In comparison, both doped PMMA preforms (PM02, PM05) show a higher T_g, by ≈+10 °C, than the undoped PM00. This could indicate that the mobility of the PM00 chain segments decreases upon charging with WO_3 during radical polymerization, i.e., PMMA/WO_3 composite preforms become more rigid than the pure PMMA preform.

Some organic/inorganic composites have also been known to show trends similar to the ones reported here in the glass transition increment upon doping with various nanoparticles.[45] Hammani et al.[46] showed an enhancement in T_g by up to 60 °C with increasing ZnO NPs loading in PMMA matrix from 0 to 40%wt. They found that the dispersion of ZnO NPs in the PMMA matrix hinders the movement of macromolecules and increases the T_g of the sample. In another study, Nikolaidis et al.[26] attributed the increase of T_g of nanocomposites (PMMA/Cloisite) to their higher molecular weight distribution than the pure PMMA.

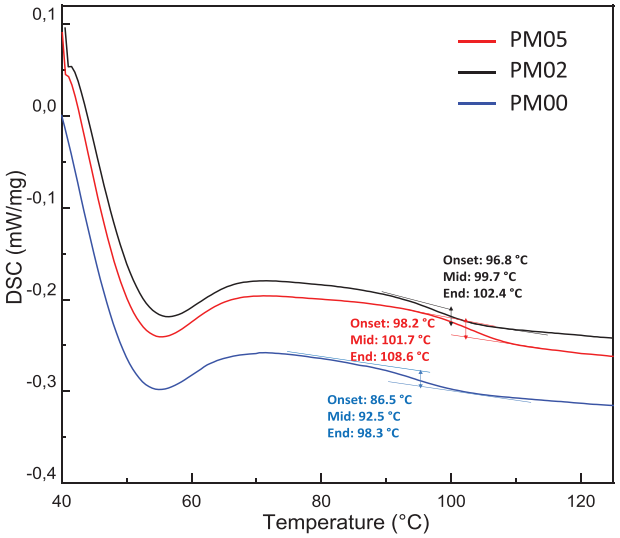

Figure 2. DSC curves of the hybrid WO_3-doped PMMA preforms.

3.2.2. Melt Flow Index

MFI of polymers was measured to provide more details on the flow behavior of the preforms, which is a valuable information for their usability in fiber drawing. MFI gives insight into the molecular weight distribution (MWD) of polymer chains and the weight ratio of the flow rate of polymers over a specific time and temperature range.[47] Hence, the polymer composite with lower MFI (low flow) has longer chains and higher MWD. Table 1 indicates the flow properties of PMMA/WO_3 preforms. PM00 exhibits a melt flow index value of 15.5 g 10 min^{-1} which is close to the commercial values of the PMCom (17.5 g 10 min^{-1}). With that respect, this is important to highlight that the PMCom preform could be shaped into fiber. Hence, we consider its MFI value as a reference for the fiber drawing ability of the lab-made preforms. It is observed that the MFI decreases with the insertion of WO_3 in the PMMA, from 15.5 (0% wt. WO_3) to 13.88 g 10 min^{-1} (0.5% wt. WO_3), which may be linked to the reduced fluidity of the polymer chains as a result of the addition of NPs. Similar trend was observed by El Hady et al.,[48] as they reported that the addition of fillers (0.5% wt. of organoclay) in cross-linked polyethylene decreased the MFI from 6.46 to 1.21 g 10 min^{-1}. They explained that the MFI decrease may be traced to flow hindrance by the organoclay particles. Based on MFI conclusion, in order to maintain a good drawing ability, we selected the PM02 preform (0.2% wt. WO_3) for further study into fiber and fabric shapes.

Table 1. Glass transition temperature and melt flow index for the WO_3-doped PMMA preforms.

Sample ID	T_g [°C]	MFI [g 10 min^{-1}]
PM00	86.5	15.5 ± 0.22
PM02	96.8	13.25 ± 0.12
PM05	98.2	13.88 ± 0.42
PMCom	90.4	17.5

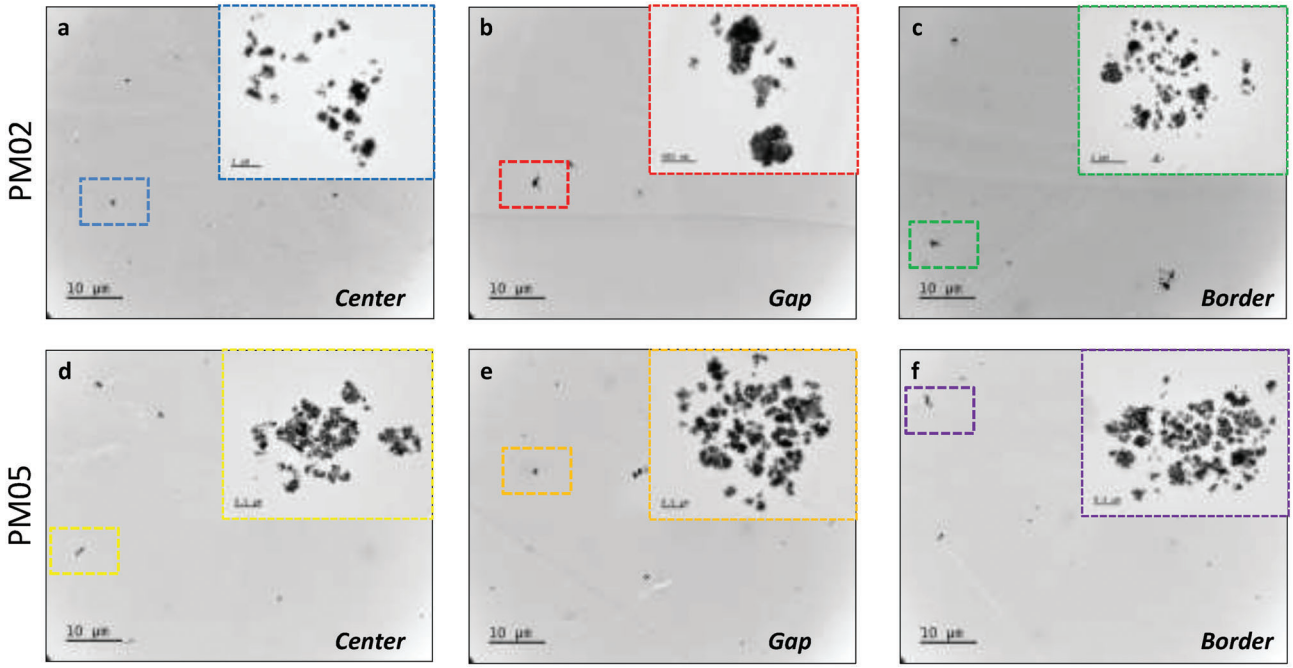

Figure 3. TEM micrographs in a) center b) gap and c) border section of the PM02 sample, and in d) center, e) gap and f) border section of the PM05 sample (inset: marge magnification on aggregates).

3.2.3. WO_3 Particle Size Distribution Inside Preforms

High-resolution transmission electron microscopy (HR-TEM) was performed to provide more insights into the dispersity of the NPs inside the polymerized transparent preform. To ensure a complete scan of the preforms slices, all measurements were observed in three different areas, from center, to gap (in between border and center) to border (**Figure 3**). The slices observed by HR-TEM had a thickness of 70 nm for a surface of 300 × 300 nm^2. All of them exhibit phase-separated WO_3 NPs agglomerates embedded in PMMA matrix, both for the PM02 and PM05 compounds (Figure 3, upper and lower panels respectively). Despite slight phase separation, the PM02 keeps a good transparency with no visual defects or macro bubbles, while the PM05 exhibits a homogeneous opaque blue coloration with no visual defects.

Particles are grouped in large agglomerates consisting of separated groups of lower-size aggregates, following a fractal organization, as depicted in the inset of Figure 3. The strongly inhomogeneous distribution of the NPs domains makes such statistical study very challenging. With this limitation said an attempt for a detailed statistical study of the average size of the aggregates using Image-J software is proposed as Supporting Information. The length of the lower-size individual aggregates in each section for PM02 and PM05 is averaged on three different aggregate regions. This approximation gives a clear vision about the length/size of aggregation in each domain. From the histograms in the Supporting Information and Figure 3a–c, the average length of the aggregates in PM02 in the border section (374 ± 47 nm) is higher than the center (262 ± 52 nm) and again higher than in the gap sections (181 ± 38 nm). As shown in Figure 3d–f, the aggregations in PM05 record larger overall size: borders (408 ± 32 nm), center (312 ± 28 nm), and gap (358 ± 44 nm). The formation of aggregations was previously observed by Wegener et al.[44] in PMMA-doped with ZnO NPs by bulk radical polymerization, where they reported on the polymerization-induced segregation of the primary particles to form domains within the bulk polymer. In another study, Xu et al.[49] prepared PMMA-based nanocomposite films with ultra-high-loading ZnS quantum dots via bulk thermo-curing copolymerization method. Here also, they noticed the formation of aggregates and irregular phase domains in the PMMA/ZnS nanocomposites.

3.2.4. Photochromic Study of the Doped Preforms

The PM02 preform was selected to study photochromic properties as it maintains good transmission properties close to the PM00 associated with proper thermal drawing ability. A 1 mm slice was cut from the PM02 preform and employed for photochromic study using Halon as white reference. Ex situ diffuse reflectance (R%) measurements were performed after 2, 4, 8, 15, 25, 45, 60, and 90 min of irradiation (**Figure 4**a) on the preform slice deposited on a 100% reflective white background. Hence, its reflectance can be in first approximation (i.e., considering that scattering phenomena from the WO_3 particles have a negligible effect on the signal) complementary to the WO_3 absorbance. The reflectance of the PM02 versus UV-light irradiation time on the 450–2200 nm wavelength range was recorded and transformed in Kubelka–Munk absorbance spectra ($K/S = (1-R)^2/(2 \times R)$).[50] The K/S transform exhibits an intensity of the absorption phenomena proportional to the chromophore concentration (herein, chromophore centers into the WO_3 particles) and so are used for kinetic analysis. As shown in Figure 4a, the PM02 ex-

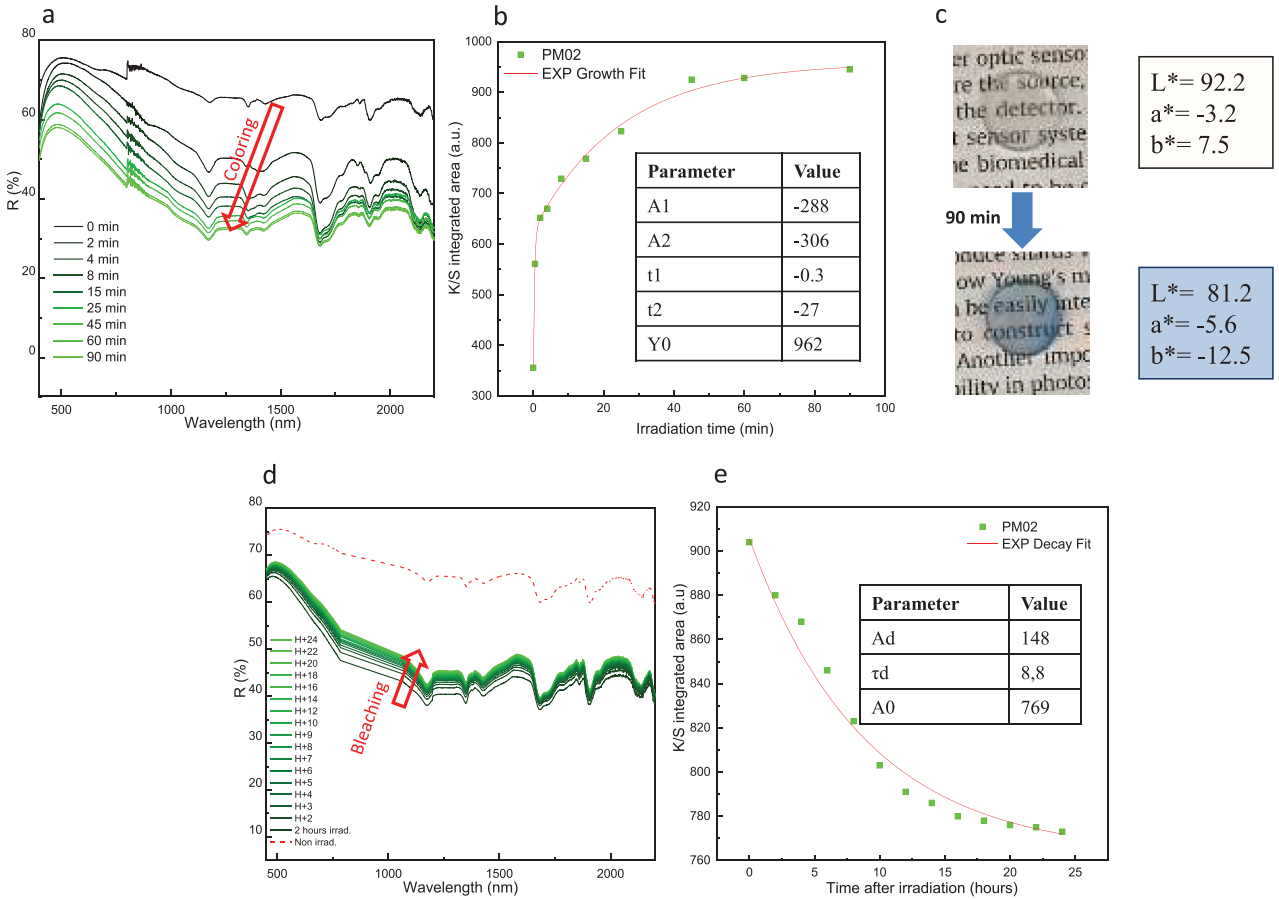

Figure 4. Photochromic reflectance spectra of the 0.2% WO_3-doped PMMA preform (PM02) versus time for a) coloring versus irradiation and d) bleaching under dark. Kinetic study based on the evolution of the average K/S absorbance (400–2500 nm): b) during coloring and e) during bleaching. c) PM02 slice before and after 90 min irradiation with the corresponding colorimetric coordinates.

hibits a photochromic effect mainly observed in the near-infrared part of the spectrum (due to the $W^{5+} \rightarrow W^{6+}$ inter-valence charge transfer responsible for the visible-NIR absorption band centered at ≈1 µm wavelength). The associated chromatic coordinates in L*, a*, and b* space are presented in Figure 4c, which quantify the photochromic efficiency of the PM02 from the optical contrast calculated between the non-irradiated and 90 min irradiated states. It allows the calculation of visible ΔC contrast: $\Delta C = \sqrt{(\Delta b^{*2} + \Delta L^{*2} + \Delta a^{*2})} = 22.9$ in between the initial and the 90 min irradiated states (a contrast above 5 becomes clearly visible by human eyes). To better express the photochromic coloring kinetic, a double exponential function (a combination of two first-order kinetic laws) was used to fit the experimental data, according to Equation (1):

$$Y = A_1 \times \exp\left(t/t_1\right) + A_2 \times \exp\left(t/t_2\right) + Y_0 \quad (1)$$

with t in min., two characteristic times (t_1 and t_2) in min., and two characteristic amplitudes (A_1 and A_2). The values of the parameters are shown in Figure 4b. Compared with our previous study on the mechanism of photochromism in WO_3-based films and powders,[38,51] we observe quite similar coloring kinetic. It consists of two kinetic phenomena with almost the same amplitude (A1 almost equal to A2): a fast-kinetic component (t_1 = 0.3 min) affecting the coloring mainly during the very first minutes, and a slow-kinetic component (t_2 = 27 min). We proposed in previous works[51] that the fast kinetic corresponds to a quick photo-reduction of the surface cations from W^{6+} to W^{5+}, then the surface becomes saturated with W^{5+} ions and this fast mechanism stops. The slow kinetic presents the ionic diffusion of the W^{5+} from the surface to the material bulk, allowing W^{5+} surface desaturation and so new surface photoreduction.

For the bleaching study, the 90 min irradiated PM02 slice was left in the dark for self-bleaching, directly in the spectrometer chamber, automatically recording the evolution of the reflection spectra for 24 h. In a similar manner than for coloring study, the reflection spectra in Figure 4d were transferred to K/S and shown in Figure 4e. The gap between the spectrum obtained after 24 h darkening and the spectrum of the initial state remains important. The reflectance contrast (ΔR), taken as equal to the reflectance difference in IR range at 1200 nm between the 24 h bleached sample (H+24) and the initial state (90 min just irradiated) shows that the reversibility rate is only ≈21% (percentage calculated from the ratio between the H+24 and the initial states).

Table 2. Calculated and measured diameters of the issued WO_3-doped PMMA fibers.

Fibre		T_{draw} [°C]	V_{feed} [mm min^{-1}]	V_{draw} [m min^{-1}]	D_{pref} [mm]	D_f [µm] calculated	D_f [µm] measured
FPM00	Large	124	1	0.5	12	537	550 ± 50
	Thin	124	1	4	12	190	145 ± 15
FPM02	Large	138	1	0.5	12	537	420 ± 40
	Thin	138	1	6	12	154	135 ± 15
FPM05	Large	142	1	0.5	12	537	620 ± 60
	Thin	142	1	1	12	379	385 ± 40

For the bleaching kinetic, the fitting of the experimental data was achieved using a single decay component following Equation (2):

$$Y = A_d \times \exp(-t/\tau_d) + A_0 \quad (2)$$

with τ_d : the characteristic bleaching time in hour. In this case, the A_d and A_0 fitting parameters has poor physical signification since the bleaching is not complete. Nonetheless, the A_d/A_0 ratio, equal to 20%, is directly associated with the fitted reversibility rate. The phenomenon of re-oxidation of W^{5+} to W^{6+} by the oxygen in the air is predicted to be very slow compared to photoreduction of W^{6+} to W^{5+} under UV irradiation.[38,51] τ_d is 8.8 h. Hence, we can conclude that the PM02 preform shows a poor bleaching behavior at room temperature, with very slow kinetic and uncompleted reversibility.

Many researches in photochromic composite compounds confirm that oxygen molecules improve the bleaching of the WO_3-based composite, which can be accomplished by the oxidation of the W^{5+} metal centers (at the origin of the blue coloration) from electron transfer from the +V metal ions to the oxygen molecules.[52] Oxygen can be mainly provided from polymers with enough OH groups such as vinyl polymers,[53] nano cellulose,[35] and hydrogel[54] However, since the proposed hybrid PMMA/WO_3 contains many structural C═O groups and insufficient OH groups, such polymeric matrix can block rapid spontaneous reoxidation and stabilize the blue coloration.[55] Noteworthy, the bleaching behavior of WO_3-based materials can be improved by heating the material to 80–100 °C in air or under ozone (oxidative conditions) to obtain a complete relaxation.[36] This route was not investigated as it is outside of the scope of this study. Hereafter, we will show that the blocking effect of the polymeric matrix besides the bleaching behavior is drastically limited for shaped fibers.

3.3. Single Fiber Characterization

3.3.1. Aspect Ratio of the Fibers

Following, the preforms were thermally stretched down into optical fibers (labeled as FPM00, FPM02, and FPM05 with respect to the WO_3 particle content). Different diameters of fibers (D_{fib}) were issued from the preform drawing process by changing the preform feed velocity (V_{feed}) or/and the fiber drawing velocity (V_{draw}). The diameter of the lab-made PMMA fibers can be theoretically calculated with respect to the preform diameter (D_{pref}) using the equation of mass conservation[56] (Equation (3)):

$$\frac{D_{pref}^2}{D_{fib}^2} = \frac{V_{draw}}{V_{feed}} \quad (3)$$

A thin and a large diameter fibers were stretched down from each of the three preforms. The drawing parameters (T_{draw}, V_{feed}, V_{draw}, and D_{pref}), along with the calculated and measured diameters are listed in **Table 2** with varying drawing velocities. For each change in V_{draw}, measurement of D_{fib} was performed (afterward using the optical microscope) on fully stabilized sections of fibers, as an average of 3 meters of fiber is needed to reach again a uniform section.

The increase of the recorded drawing temperature with the increase of the tungsten oxide content is in good agreement with the variation of the T_g, which increases upon doping with WO_3 due to the blocking of the chain segments of PMMA. Furthermore, the calculated diameters are found relatively close to the measured ones (accuracy estimated ≈10%), which confirms the feasibility of fiber diameter control by drawing parameters.

The SEM analysis in cross-sectional and longitudinal views of the lab-made PMMA/WO_3 hybrid FPM00, FPM02, and FPM05 fibers are shown in **Figure 5**. The fiber sample FMP00 (Large) was embedded in an epoxy resin, the surface was then polished to improve the visualization of the cross-section (Figure 5a). The samples FPM02 and FPM05 were cut by a diamond cleaver and fixed vertically facing the SEM detector (Figure 5b). For all samples observed in longitudinal view, the SEM images indicate a good surface quality (Figure 5c–e). No surface imperfection (micro cracks, pores, defects) could be detected on the cross-section or surface of the fibers. The six studied fibers cannot be differentiated neither by visual inspection nor by SEM images due to the nanometric doping that cannot be tracked using the SEM device resolution.

3.3.2. Optical Signal Quality: Attenuation of the Fibers

Attenuation measurement in optical fibers was recorded using the well-established cut-back method. The attenuation coefficient is defined as the logarithm relationship between the transmitted input power P(0) and the output power P(x) observed after propagation of a distance x in an optical fiber system (Equation (4))[57]:

$$\alpha_{total}\,(dB/km) = (10/x) \times \mathrm{Log}\,[P\,(0)\,/\,P\,(x)] \quad (4)$$

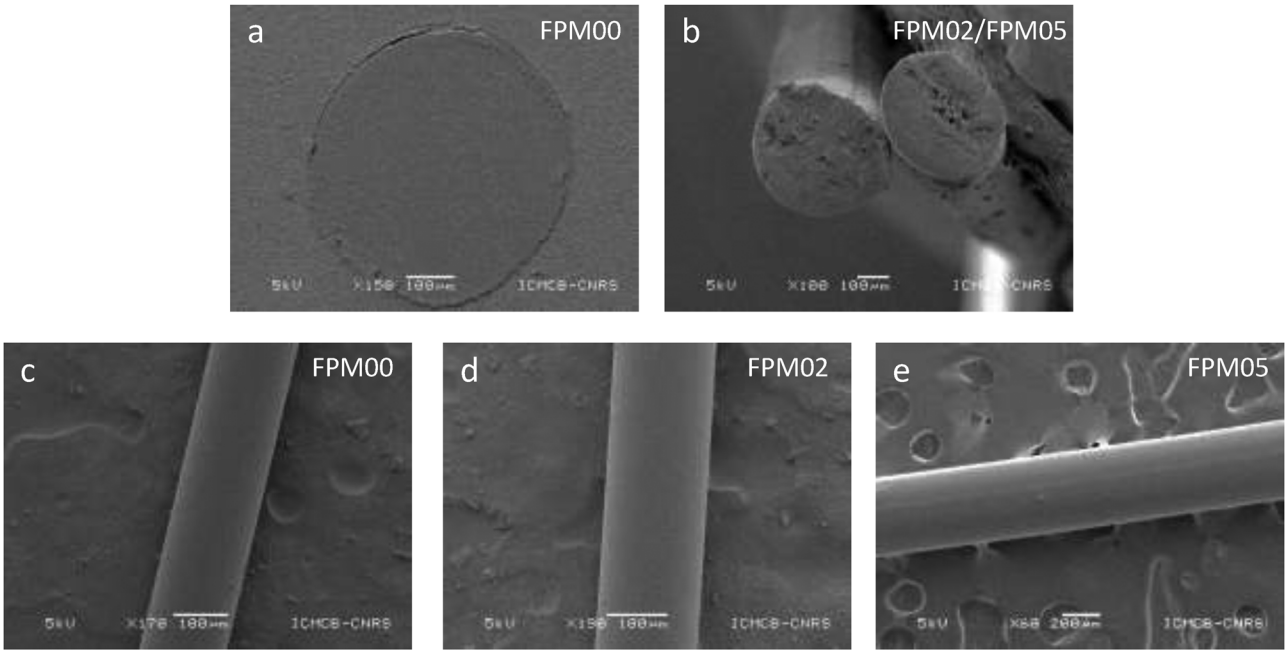

Figure 5. SEM micrographs of lab-made WO_3-doped PMMA hybrid fibers. Cross-sectional views of a) FPM00, b) FPM02 and FPM05 fibers. Longitudinal views of c) FPM00, d) FPM02 and e) FPM05 fiber.

This equation is known as Beer's Law and clearly shows that the power of the transmitted signal decreases exponentially with the propagated distance. Using Equation (4) the attenuation of the FPM00, FPM02, and FPM05 fibers (thin diameters) has been measured in the range 450–850 nm (**Figure 6**). A commercial PMMA fiber (labeled as FPMC) provided by *XLY Fiber company* ($D_f = 350$ µm) was used as a reference.

As shown in Figure 6c, the attenuation curves of the lab-made fibers exhibit a similar shape to the commercial fiber, yet with higher loss level. Attenuation in PMMA can be caused by intrinsic or extrinsic loss. Intrinsic loss mechanisms result from the chemical and physical structure of the PMMA fiber. First types are the absorption losses, which mainly consist of the molecular vibrational absorption of the C—H bonds and of the absorption due to electronic transitions between different energy levels within the molecular bonds.[58] The C—H vibrational absorption can be observed at higher wavelengths as shown at the local maximum (732 nm) that increases from 4.2 dB m^{-1} in FPMC to 6.7 dB m^{-1} in FPM05. Also, extrinsic loss mechanism can originate from absorption by contaminants, water, or extrinsic doping materials (herein WO_3) incorporated in the fiber.[59,60]

Second types are caused by Raleigh/Mie scattering occurring from the WO_3 nanoparticles, dust inclusions, microporosity, or even density and composition fluctuations in the PMMA

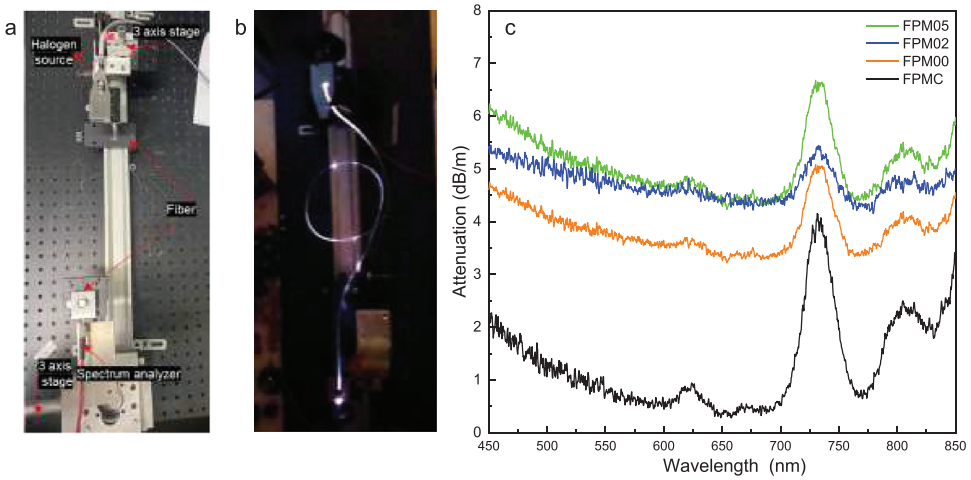

Figure 6. Loss measurements on the WO_3-doped PMMA hybrid fibers a) Photography of the cut-back measurement set up, b) A 2.5-meters-long FPM02 fiber excited by the Halogen lamp under dark conditions, c) Loss spectrum (attenuation factor) of the lab-made PMMA/WO_3 thin fibers with various WO_3 content along and comparison with a commercial PMMA fiber (FPMC).

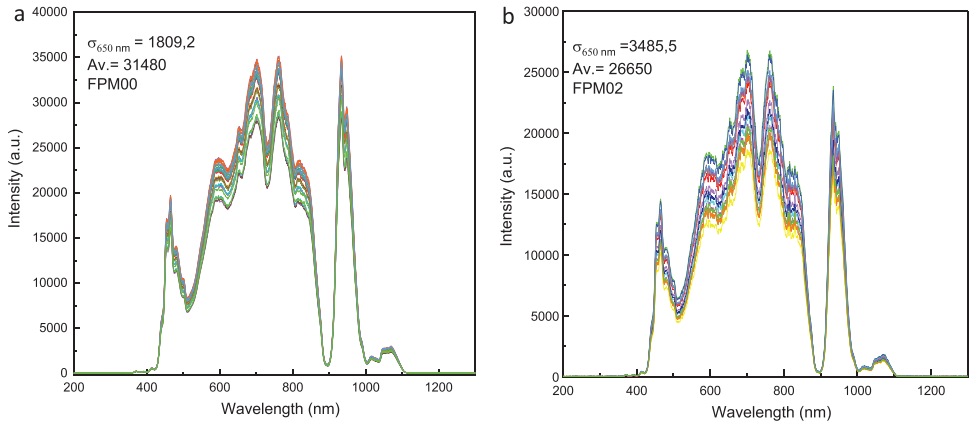

Figure 7. Optical transmission signal intensity variations for 15 cuts of the lab-made PMMA optical fibers a) FPM00 fiber and b) FPM02 fiber.

polymer. Rayleigh scattering happens when the scattering source diameter is at least ten times smaller than the wavelength of the light.[61] Meanwhile, Mie scattering occurs when the particle diameter is equal or higher to the wavelength of light.[62] Rayleigh scattering occurs at all the wavelengths, but with a clear decrease of its intensity versus wavelength increase whereas Mie scattering efficiency is negligibly depending on wavelength. Since the size of the incorporated WO_3 particles varies between 200 and 5000 nm, as predicted from the size of aggregation inside the preforms, both Rayleigh scattering and Mie scattering can occur inside the fibers. This confirms the fact that WO_3 particles are expected to play a dual role as scattering and absorption centers leading to increased optical loss in comparison with undoped PMMA fibers. Here the amplified attenuation with the WO_3 doping originates from both the scattering and the absorption properties of WO_3 particles.

3.3.3. Optical Signal Quality: Reproducibility of the Transmission Measurements

In the following section, we mainly focus on the FPM02 hybrid fiber since it exhibits a lower attenuation than the FPM05 fiber, which makes it a better candidate for the desired optical application. Two new samples: a 0.2 wt.% doped and an undoped sample were prepared; in order to eliminate any external effects on the consistency of the measurements the fibers were produced in the same drawing conditions ($V_f = 1$ mm min^{-1}, $V_d = 2$m min^{-1}, with 275 ± 25 µm diameter) and the entrance and end faces of each pieces were polished in the same manner. First, in order to assess the longitudinal homogeneity of the lab-made FPM00 and FPM02 fibers, we recorded the transmission signal of 15 different 5-cm-long cuts. As can be seen in **Figure 7**a, the transmitted signal through the 15 different cuts of a FPM00 fiber superimposed relatively well, with an average maximum transmission intensity of 31 480 and a standard deviation of 1809. In comparison, the transmitted signal through the 15 cuts of the FPM02 fiber exhibits a lower maximum 26 650 and a higher standard deviation of 3485 (Figure 7b).

It appears that the incorporation of the WO_3 NPs within the PMMA fiber leads both to a decrease in the total transmitted optical signal and a deterioration of the signal homogeneity along the fiber. This result could be predicted since the WO_3 NPs act as extrinsic scattering and absorption centers. Nevertheless, within these limitations, the quality of the transmitted signal remains steady and significantly high for both fibers, assessing our protocol for the elaboration of hybrid WO_3/PMMA fibers.

3.3.4. Photochromic Properties of Single Plastic Fibers (Axial Transmission)

Samples with a length of 5 cm (diameter of 275 µm) were used to evaluate the photochromic properties of the FPM02 fiber. The fiber was irradiated from the side using a UV lamp of 8 W, the power per surface unit received by the sample being equal to 5.6 W m^{-2}. The use of such low fluence is choice to mimic the real condition in which a smart device (window or textiles) is exposed in daily light. The evolution of the transmission spectrum of the FPM02 versus irradiation time is depicted in **Figure 8**a. The maximum intensity evolution at 650 nm was extracted to investigate further the photo-redox kinetic (Figure 8b). Upon irradiation, the transmitted signal quickly degrades as a result of the increased absorption of WO_3 NPs under UV excitation. The tungsten oxide acts as an absorption center, leading to an increased transmission loss. As shown in Figure 8c, the color of the FPM02 fibers (single fiber and bundle) turned from transparent to blue after 1 h of irradiation. Consistently with the previous study on the WO_3-doped preform slices, the coloring kinetic is expressed by a double exponential function as Equation (1).

Fitting of the experimental data according to Equation (1) is depicted in Figure 8b. The maximum intensity of FPM02 drops rapidly in the first 15 min of irradiation, then it slowdowns beyond 15 min of irradiation, until almost no longer evolving after 120 min. We calculate from Equation (1) that the coloring kinetic consists of two kinetic phenomena: a fast-kinetic component (A1 = 6340, $t_1 = 4$ min) and a slow kinetic component (A2 = 20 417, $t_2 = 48$ min). In fibers, as it was already the case for the preforms, the coloring kinetic seems mainly governed by the kinetic of WO_3, as reported in our last papers,[36,38] which confirms weak effect of the PMMA matrix on photochromism (for the coloring mechanism). It can however be noticed that, because of different

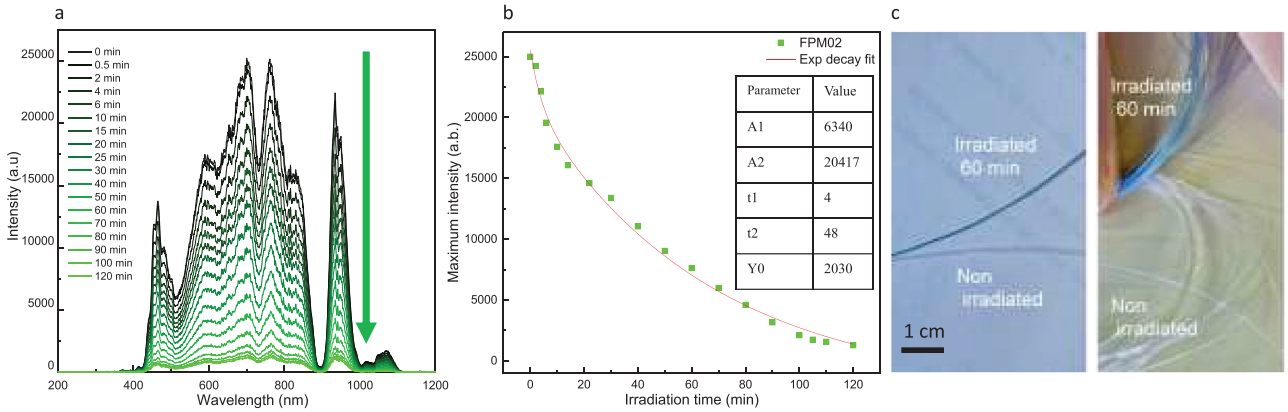

Figure 8. Photochromic coloring of the 0.2% WO_3-doped PMMA fiber (FPM02). a) Axial transmission spectra versus irradiation times, b) Kinetic study based on the transmission intensity (at 650 nm) versus irradiation time, c) Photographs of a single fiber and of a bundle of FPM02 fibers before and after irradiation.

shape and especially a different surface/volume aspect-ratio, the two characteristic times t_1 and t_2 describing the coloring kinetic are both increased for fibers versus preforms (the signal for fibers is measured in transmittance while it is in absorbance for the preforms, which leads to a sign inversion of the characteristic times). Our hypothesis to explain the slower coloring of fibers compared to preform is a lesser efficiency of the irradiation in the fiber case due to its cylindrical aspect.

The same pre-irradiated FPM02 fiber was used for bleaching study (**Figure 9**). The fiber was left in the dark at room temperature for self-bleaching using the same set-up while automatically recording the evolution of the transmission signal. Unlike observations made on the PM02 preform (Figure 4), the FPM02 shows a reversible and almost complete bleaching mechanism, returning to its transparent appearance after 24 h in the dark (Figure 9a). The maximum transmission intensity evolution can be fitted from a single exponential growth trend on the complete 20 first-hour range, according to Equation (2) already used on preform slices. Beforehand, the bleaching mechanism is governed by the phenomenon of reoxidation of W^{5+} to W^{6+} by the oxygen from the atmosphere. We assume that the principle change from preform to fiber is again their aspect-ratio. Considering aspect-ratio, the evolution of diameter from preform to fiber is given by: D_p/D_f = 12 000/265 µm = 45.3, which we believe leads to an higher proximity of the WO_3 nanoparticles to the fiber surface and so the oxidizing atmosphere. Actually, the bleaching kinetic of the fibers is nearly close to the one of WO_3 powder beds, reported in previous works.[34] This confirms that the slower and partially non-reversible bleaching only observed for the preforms was due to the « optical passivation » of the dispersed particles in the PMMA matrix, which is poorly oxygen diffusive, i.e., the PMMA matrix in preform (thick) geometry tends to prevent the redox reaction at the origin of the WO_3 particle photochromism.

This set of experiments shows a huge optical contrast of the hybrid fibers between the colored and bleached states, that is to

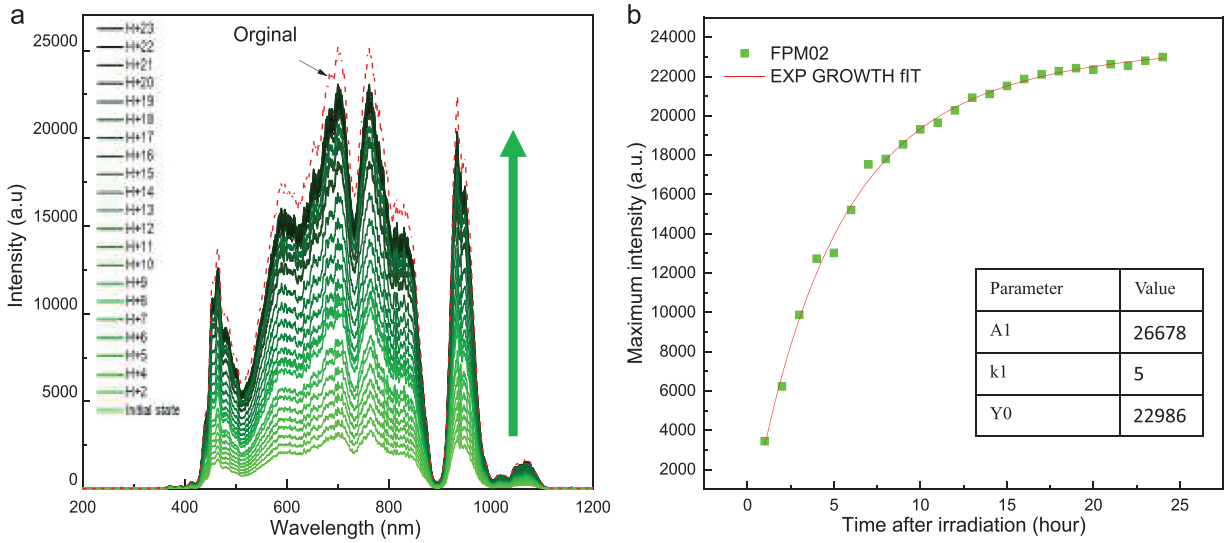

Figure 9. Photochromic bleaching under dark of the 0.2% WO_3-doped PMMA fiber (FPM02). a) Evolution of axial transmission signal in dark conditions, b) kinetic study based on the transmission intensity (at 650 nm) versus time after irradiation.

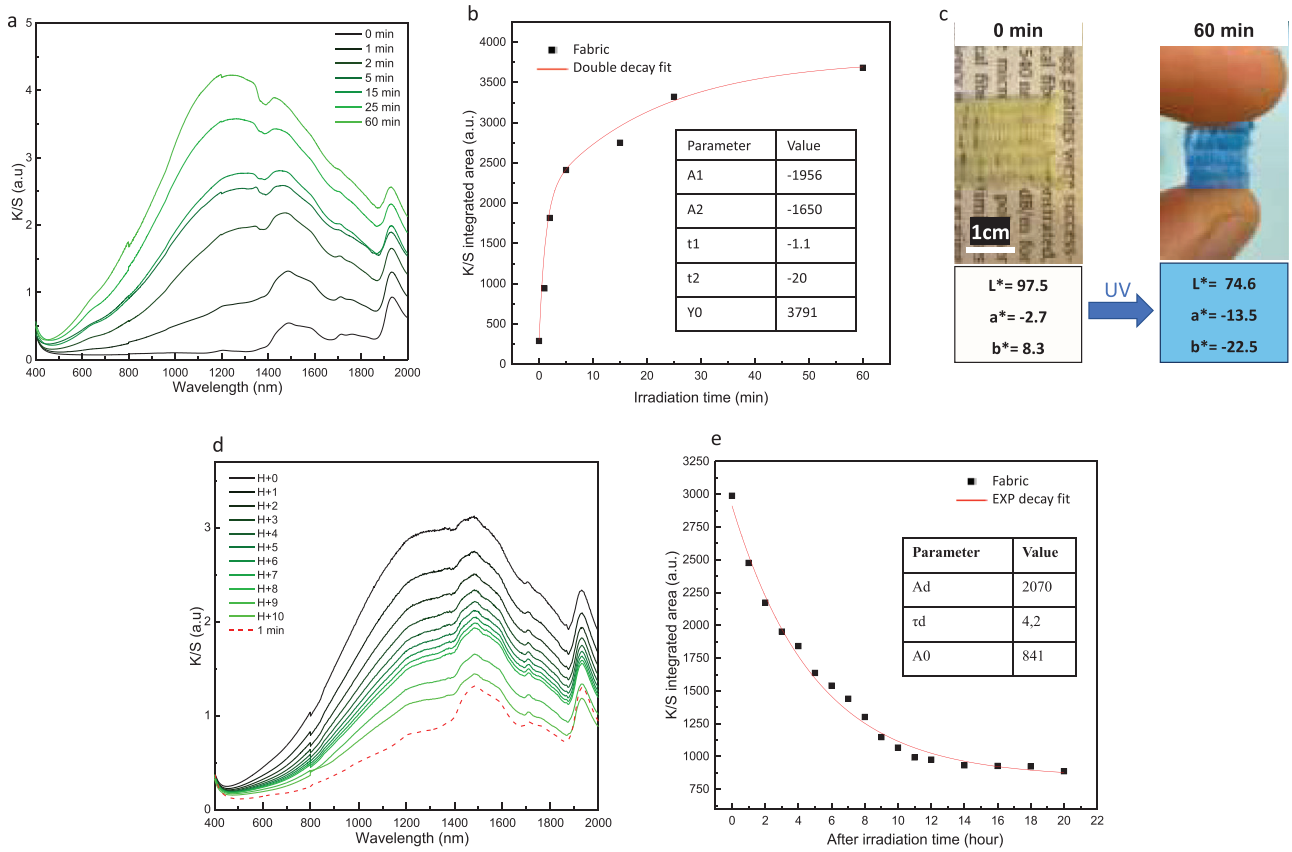

Figure 10. Photochromic K/S spectra of a 2D fabric made of 0.2% WO_3-doped PMMA fibers (PM02) versus time for a) coloring versus irradiation and d) bleaching under dark. Kinetic study based on the evolution of the average K/S absorbance (400–2500 nm): b) during coloring and e) during bleaching. c) Photographs of the fabric before and after irradiation with the corresponding colorimetric coordinates.

say the axial transmission of the fiber is nearly turned-off during the NPs coloring step (under UV irradiation) while it is nearly full recovery during the NPs bleaching step. It constitutes a rare example of a positive (enhancement) change of the photochromic properties with the effect of the shaping of the material, here from the NPs to the preforms then to the 1D fibers.

3.4. Photochromic Properties of 2D Textile

In this section, we discuss the optical properties of a 2D system consisting of photochromic pieces of FPM02 fibers woven manually into a fabric with dimension 2×2 cm^2 (**Figure 10**). The fibers were selected from the same fiber drawing section with similar diameter. Ex situ diffuse reflectance (%R) of the fabric after exposure of 1, 2, 5, 15, 25, and 60 min under UV lamp (8 W) were recorded and the results are presented in Figure 10a.

Comparing to other researches in the field, Bao et al.[63] produced photochromic cotton fabric via thiolene click chemistry using the spiropyrane derivatives as the photochromic active part. The synthesized photochromic materials show a good color-changing rate and fading rate with visible contrast ≈50 between non-irradiated and irradiated states. Notably, our 2D fabric exhibits a quick response after 1 min of irradiation, as proved from the quick degradation of the reflectance curve between 0 and 1 min. The coloring kinetic was evaluated by fitting the experimental data using a double exponential function according to Equation (1) (Figure 10b) (based on the K/S absorption spectra which is a most adequate representation of the color evolution for the 2D fabric). In the case of the fabric, the two kinetic phenomena show almost the same amplitude (A_1 almost equal to A_2) with $t_1 = 1.1$ min $t_2 = 20$ min. The associated chromatic coordinates in L*, a*, and b* space are calculated for the 0 and 60 min irradiated states (Figure 10c). The visible ΔC contrast is found to be: $\Delta C = \sqrt{(\Delta b^{*2} + \Delta L^{*2} + \Delta a^{*2})} = 43.6$. Indeed, the textile gives a very good color contrast, which is important for application as a smart textile. Hence, in terms of kinetic and contrast, the 2D textiles exhibit the quickest and deepest coloring properties. The slight improvement in comparison with the coloring of a single fiber from its axial transmission is surely due to the capacity of the textile to intercept efficiently the UV irradiation from the UV lamp. Hence, the shaping step to applicative manufactured 2D products, with large surface/thickness ratio is associated with improved photochromic coloring.

For the bleaching study, the irradiated fabric investigated above was left in dark in the spectrometer chamber for self-bleaching. As for coloring study, the reflection spectra were transferred to K/S (Figure 10d). As expected, the fabric shows a reversible be-

havior similar to single FPM02 fibers. Bleaching kinetic was followed by recording the evolution of average K/S versus after-irradiation time (Figure 10e). The K/S evolution can be fitted from a single exponential decay trend according to Equation (2). The kinetic of the bleaching mechanism of the fabric appears to be almost the same than of the fiber FPM02: the characteristic decay time τd is equal to 4.2 h, to be compare to the one calculated for the fiber (5.0 h). Thus, the fabric exhibits a reversible photochromism, returning to almost its initial state for 20 h (with >90% recovery after 8 h), that is, one night is sufficient for reinitializing and re-using the as-prepared smart textile.

4. Conclusion

In this work, we have investigated the elaboration and photochromic properties of hybrid inorganic/organic WO_3-doped PMMA optical fibers. Macroscopic preforms have been successfully synthesized by the radical polymerization of MMA-doped with modified photochromic WO_3 nanoparticles, followed by their thermal stretching into tens-of-meters-long optical fibers with diameter ranging 200–600 µm. The 0.2% WO_3-doped preform shows a slow coloring mechanism and an irreversible photochromic behavior while single fibers exhibit more intense and more rapid coloring and bleaching phenomena, comparable to the phototochromic parameters of WO_3 powder beds. This shows that, even if the PMMA matrix contributes to block the oxygen diffusion as the source of the WO_3 redox activity and color changes, the design of thin composite fibers enables the redox photochromic activity of the embedded WO_3 nanoparticles with large optical contrasts. Moreover, we have presented a hand-made 2D photochromic fabric made with 0.2%-WO_3-doped fibers. It shows a fast bleaching response, with a decay time of 4.2 h, along with a very large visible contrast ($\Delta C = 43.6$). The proposed hybrid WO_3/PMMA composites are thermally stable and amenable to shaping, without compromising the sensitivity of their photochromic phenomena. The successful coloring/bleaching mechanism of the proposed 1D single fibers and 2D fabric systems, conjugated to a fast response to UV excitation, demonstrates their potential as flexible fiber-based UV-sensor devices and smart textiles.

Supporting Information

Supporting Information is available from the Wiley Online Library or from the author.

Acknowledgements

The authors acknowledge the support from the University of Bordeaux and from the LIGHT S&T Graduate Program (PIA3 Investment for the Future Program, ANR-17-EURE-0027). The authors acknowledge Antony Chiron and Alexandre Fargues for helpful contributions.

Conflict of Interest

The authors declare no conflict of interest.

Data Availability Statement

The data that support the findings of this study are available from the corresponding author upon reasonable request.

Keywords

photochromic fibers, plastic optical fibers, poly(methyl methacrylate) (PMMA), smart textiles, tungsten oxide

[1] S. Parola, B. Julián-López, L. D. Carlos, C. Sanchez, *Adv. Funct. Mater.* **2016**, *26*, 6506.
[2] M. Faustini, L. Nicole, E. Ruiz-Hitzky, C. Sanchez, *Adv. Funct. Mater.* **2018**, *28*, 1704158.
[3] B. Kumar, B. K. Kaushik, Y. S. Negi, *Polym. Rev.* **2014**, *54*, 33.
[4] J. Lee, B. Llerena Zambrano, J. Woo, K. Yoon, T. Lee, *Adv. Mater.* **2020**, *32*, 1902532.
[5] Y. Weng, Z. Yu, T. Wu, L. Liang, S. Liu, *New J. Chem.* **2023**, *47*, 5086.
[6] R. R. Søndergaard, M. Hösel, F. C. Krebs, *J. Polym. Sci., Part B: Polym. Phys.* **2013**, *51*, 16.
[7] J. Zubia, J. Arrue, *Opt. Fiber Technol.* **2001**, *7*, 101.
[8] K. Makino, Y. Akimoto, K. Koike, A. Kondo, A. Inoue, Y. Koike, *J. Lightwave Technol.* **2013**, *31*, 2407.
[9] Y.-G. Nan, D. Kinet, K. Chah, I. Chapalo, C. Caucheteur, P. Mégret, *Opt. Express* **2021**, *29*, 25824.
[10] S. Shabahang, S. Forward, S.-H. Yun, *Opt. Express* **2019**, *27*, 7560.
[11] M. S. Moslan, M. H. D. Othman, A. Samavati, M. A. M. Salim, M. A. Rahman, A. F. Ismail, H. Bakhtiar, *Opt. Fiber Technol.* **2020**, *55*, 102162.
[12] C. Marques, A. Pospori, G. Demirci, O. Çetinkaya, B. Gawdzik, P. Antunes, O. Bang, P. Mergo, P. André, D. Webb, *Sensors* **2017**, *17*, 891.
[13] I. Mollers, D. Jager, R. Gaudino, A. Nocivelli, H. Kragl, O. Ziemann, N. Weber, T. Koonen, C. Lezzi, A. Bluschke, S. Randel, *IEEE Commun. Mag.* **2009**, *47*, 58.
[14] S. Abrate, R. Gaudino, G. Perrone, *Current Developments in Optical Fiber Technology*, InTech, London, UK **2013**.
[15] B. Gauvreau, N. Guo, K. Schicker, K. Stoeffler, F. Boismenu, A. Ajji, R. Wingfield, C. Dubois, M. Skorobogatiy, *Opt. Express* **2008**, *16*, 15677.
[16] B. Harsanto, I. Primiana, V. Sarasi, Y. Satyakti, *Sustainability* **2023**, *15*, 1549.
[17] T. V. Pinto, D. M. Fernandes, A. Guedes, N. Cardoso, N. F. Durães, C. Silva, C. Pereira, C. Freire, *Chem. Eng. J.* **2018**, *350*, 856.
[18] A. Charas, A. L. Mendonça, J. Clark, J. Cabanillas-Gonzalez, L. Bazzana, A. Nocivelli, G. Lanzani, J. Morgado, *Front. Optoelectron. China* **2010**, *3*, 45.
[19] J. Arrue, F. Jiménez, I. Ayesta, M. A. Illarramendi, J. Zubia, *Polymers* **2011**, *3*, 1162.
[20] P. Miluski, *Fibers* **2017**, *5*, 15.
[21] C. Jiang, M. G. Kuzyk, J.-L. Ding, W. E. Johns, D. J. Welker, *J. Appl. Phys.* **2002**, *92*, 4.
[22] P. Stajanca, I. Topolniak, S. Pötschke, K. Krebber, *Opt. Fiber Technol.* **2018**, *41*, 227.
[23] P. Miluski, M. Kochanowicz, J. Zmojda, D. Dorosz, *Spectrochim. Acta, Part A* **2018**, *192*, 88.
[24] P. Miluski, M. Kochanowicz, J. Zmojda, D. Dorosz, *Photonics Lett. Pol.* **2017**, *9*, 110.
[25] M. E. El-Hefnawy, A. I. Ismail, M. I. Orif, S. T. Al-Goul, A. Elmushyakhi, M. Abou Taleb, *Luminescence* **2023**, *38*, 1358.
[26] A. K. Nikolaidis, D. S. Achilias, G. P. Karayannidis, *Ind. Eng. Chem. Res.* **2011**, *50*, 571.
[27] I. Parola, E. Arrospide, F. Recart, M. Illarramendi, G. Durana, N. Guarrotxena, O. García, J. Zubia, *Fibers* **2017**, *5*, 28.

[28] L. Jaramillo-Ochoa, R. Narro-García, M. A. Ocampo, R. Quintero-Torres, *J. Lumin.* **2017**, *184*, 205.
[29] Y. Badour, V. Jubera, I. Andron, C. Frayret, M. Gaudon, *Opt. Mater.: X* **2021**, *12*, 100110.
[30] S. Zeb, G. Sun, Y. Nie, H. Xu, Y. Cui, X. Jiang, *Mater. Adv.* **2021**, *2*, 6839.
[31] P. Talvenmaa, *Introduction to chromic materials in "Intelligent Textiles and Clothing"*, Elsevier, Amsterdam, The Netherlands **2006**, pp. 193–205.
[32] H. C. Dunn, J. N. Etters, *Text. Chem. Color. Am. Dyest. Rep.* **2000**, *32*, 20.
[33] C. Avellaneda, L. Bulhoes, *Solid State Ion* **2003**, *165*, 117.
[34] M. Bourdin, M. Gaudon, F. Weill, M. Duttine, M. Gayot, Y. Messaddeq, T. Cardinal, *Nanomaterials* **2019**, *9*, 1555.
[35] O. L. Evdokimova, T. V. Kusova, O. S. Ivanova, A. B. Shcherbakov, K. E. Yorov, A. E. Baranchikov, A. V. Agafonov, V. K. Ivanov, *Cellulose* **2019**, *26*, 9095.
[36] Y. Badour, S. Danto, C. Labrugère, M. Duttine, M. Gaudon, *J. Electron. Mater.* **2022**, *51*, 1555.
[37] Y. Zhu, Y. Yao, Z. Chen, Z. Zhang, P. Zhang, Z. Cheng, Y. Gao, *Sol. Energy Mater. Sol. Cells* **2022**, *239*, 111664.
[38] Y. Badour, S. Danto, S. Albakour, S. Mornet, N. Penin, L. Hirsch, M. Gaudon, *Sol. Energy Mater. Sol. Cells* **2023**, *255*, 112291.
[39] L. Wang, H. Hu, J. Xu, S. Zhu, A. Ding, C. Deng, *J. Mater. Res.* **2019**, *34*, 2955.
[40] X. C. Song, Y. F. Zheng, E. Yang, Y. Wang, *Mater. Lett.* **2007**, *61*, 3904.
[41] S. Zhuiykov, E. Kats, B. Carey, S. Balendhran, *Nanoscale* **2014**, *6*, 15029.
[42] R. Pardo, M. Zayat, D. Levy, *Chem. Soc. Rev.* **2011**, *40*, 672.
[43] T. He, J. Yao, *Prog. Mater. Sci.* **2006**, *51*, 810.
[44] M. M. Demir, M. Memesa, P. Castignolles, G. Wegner, *Macromol. Rapid Commun.* **2006**, *27*, 763.
[45] M. Jachak, R. Bhise, A. Chaturvedi, V. Kamble, G. Shankarling, *J. Inorg. Organomet. Polym. Mater.* **2022**, *32*, 2441.
[46] S. Hammani, A. Barhoum, M. Bechelany, *J. Mater. Sci.* **2018**, *53*, 1911.
[47] K. Pal, *Compos. Commun.* **2016**, *1*, 25.
[48] S. Elhady, O. Amin, I. S. Fahim, *Int. J. Eng. Trends Technol.* **2021**, *69*, 133.
[49] J. Xu, D. Li, *Polymers* **2018**, *10*, 1217.
[50] A. Roy, R. Ramasubramaniam, H. A. Gaonkar, *J. Biomed. Opt.* **2012**, *17*, 115006.
[51] M. Bourdin, G. Salek, A. Fargues, S. Messaddeq, Y. Messaddeq, T. Cardinal, M. Gaudon, *J. Mater. Chem. C Mater.* **2020**, *8*, 9410.
[52] L.-M. Ai, W. Feng, J. Chen, Y. Liu, W.-M. Cai, *Mater. Chem. Phys.* **2008**, *109*, 131.
[53] A. L. Popov, B. Han, A. M. Ermakov, I. V. Savintseva, O. N. Ermakova, N. R. Popova, A. B. Shcherbakov, T. O. Shekunova, O. S. Ivanova, D. A. Kozlov, A. E. Baranchikov, V. K. Ivanov, *Mater. Sci. Eng., C* **2020**, *108*, 110494.
[54] O. Oderinde, O. Ejeromedoghene, G. Fu, *Polym. Adv. Technol.* **2022**, *33*, 687.
[55] D. K. Hwang, H. J. Kim, H. S. Han, Y. G. Shul, *J. Sol Gel Sci. Technol.* **2004**, *32*, 137.
[56] M. Large, L. Poladian, G. Barton, M. Eijkelenborg, *Microstructured Polymer Optical Fibres*, Springer US, Boston, MA **2008**, pp. 83–110.
[57] N. Ioannides, E. B. Chunga, A. Bachmatiuk, I. G. Gonzalez-Martinez, B. Trzebicka, D. B. Adebimpe, D. Kalymnios, M. H. Rümmeli, *Mater. Res. Express* **2014**, *1*, 032002.
[58] A. Charas, A. Mendonça, J. Clark, G. Lanzani, L. Bazzana, A. Nocivelli, J. Morgado, *Plast. Opt. Fibers Gain Switch. Proc. FP-6-026365* **2009**.
[59] A. D. Alobaidani, D. Furniss, M. S. Johnson, A. Endruweit, A. B. Seddon, *Opt. Lasers Eng.* **2010**, *48*, 575.
[60] C. Whittaker, C. A. G. Kalnins, D. Ottaway, N. A. Spooner, H. Ebendorff-Heidepriem, *Opt. Mater. Express* **2019**, *9*, 1.
[61] P. Kubelka, *J. Opt. Soc. Am.* **1948**, *38*, 448.
[62] G. Latour, M. Elias, J.-M. Frigerio, *Appl. Spectrosc.* **2009**, *63*, 604.
[63] B. Bao, S. Bai, J. Fan, J. Su, W. Wang, D. Yu, *Dyes Pigm.* **2019**, *171*, 107778.